Sensors & Actuators: B. Chemical 358 (2022) 131509

Contents lists available at ScienceDirect

Sensors and Actuators: B. Chemical

journal homepage: www.elsevier.com/locate/snb

Design of a 3D interfacial SERS liquid sensing platform based on Au-nanobones for discrimination and quantitation of quercetin loaded nanoemulsions

Cristina Montes [a,b], M. Laura Soriano [a,c], M. Jesús Villaseñor [a,d], Ángel Ríos [a,b,*,1]

[a] Department of Analytical Chemistry and Food Technology, Faculty of Chemical Science and Technology, University of Castilla-La Mancha, 13071 Ciudad Real, Spain
[b] Regional Institute for Applied Chemistry Research (IRICA), 13071 Ciudad Real, Spain
[c] Department of Analytical Chemistry, Marie Curie Building, Campus of Rabanales, University of Córdoba, E-14071 Córdoba, Spain
[d] Department of Analytical Chemistry, Industrial Engineering School, University of Castilla-La Mancha, 13071 Ciudad Real, Spain

ARTICLE INFO

Keywords:
SERS liquid sensing platform
Three-dimensional arrays
Nanometrology
Quercetin nanoemulsions
Nutritional supplements

ABSTRACT

Characterization, and discrimination between free quercetin and quercetin-loaded nanoemulsions (Q-NEs) are described, as well as the design of a plasmonic metal liquid platform for their quantitation. First, reproducible Q-NEs synthesis using GRAS (Generally Recognized as Safe) components and a low-energy method as phase inversion temperature was used. Q-NEs were fully characterized being the resulting droplet size of 73.1 ± 2.4 nm and 69.7 ± 2.3 nm by DLS and SEM, respectively, with spherical morphology and encapsulation efficiency of 96.5%. Based on UV-Vis, Raman and SERS characterization studies, a discrimination between free quercetin and Q-NEs was achieved. Secondly, a new 3D-platform was developed based on tuned gold nanorods-bone shaped with fitted aspect ratios for Q-NEs quantification without altering its native nanostructure using the enhanced stretching at 1600 cm^{-1} as analytical signal. The developed plasmonic sensing platform allows to reach intensification factors up to 10^3 and 10^5 for the target analyte and methylene blue as Raman reporter, respectively. It was also submitted to an exhaustive evaluation of analytical performance characteristics in terms of linear dynamic range (0.5 – 30 μM), detection limit (0.2 μM) with good precision (RSD = 2.6%). The nanometrological 3D SERS approach was reliably implemented and validated on commercial nutritional supplements containing declared encapsulated quercetin as nanosized formulations by means of a statistical comparison with those ones obtained by a μHPLC-DAD method.

1. Introduction

The addition of antioxidants in the food industry is a standard practice since they constitute the main way to prevent, control and reduce the oxidation of main components in assorted commercial products. However, antioxidants commonly used in the industry are synthetic compounds, such as BHT (butylated hydroxytoluene), BHA (butylated hydroxyanisole), propyl gallate and TBHQ (tert-butylhydroquinone), and their extended use can pose a potential health risk to consumers. For this reason, it is of great importance to replace them with natural antioxidants in food matrices [1]. Phenolic compounds are the greatest source of natural antioxidants; within them, flavonoids are made up of more than 6500 compounds. According to their chemical structure, they are classified mainly into flavonones, flavonols, flavanols, anthocyanidins and isoflavones. Quercetin is a natural flavonol present in many fruits and vegetables such as onions, apples, berries, nuts, seeds, barks, flowers, tea, brassica leaves, etc. Its claimed therapeutics effects include anti-cancer, anti-inflammatory, antiulcer, anti-allergic, healing, anti-diabetic, anti-obesity, and even cataract prevention. In addition, its extraordinary antioxidant activity stands out [2]. However, all these benefits have been limited when incorporating quercetin in food matrices, due to its low solubility in aqueous media at room temperature (50 μM) [3]. This problem brought a new challenge for food industries, which was solved by developing a new strategy: encapsulation procedures. These systems can be usually classified according to their composition as lipid-based nanocarriers,

* Corresponding author at: Department of Analytical Chemistry and Food Technology, Faculty of Chemical Science and Technology, University of Castilla-La Mancha, 13071 Ciudad Real, Spain.
E-mail addresses: qa2sodom@uco.es (M.L. Soriano), Angel.Rios@uclm.efs (Á. Ríos).
[1] ORCID: http://orcid.org/0000–0003-1728–3097

https://doi.org/10.1016/j.snb.2022.131509
Received 5 December 2021; Received in revised form 19 January 2022; Accepted 29 January 2022
Available online 1 February 2022

polysaccharide-based and protein-based ones [4,5]. Until date, there have been numerous studies in which quercetin has been encapsulated in different lipid nanocarrier formulations, thus improving their bioavailability, for instance nanoemulsions [1,2,6–8], nanoliposomes [9,10], lipid nanoparticles [11–13], etc. These nanotechnological solutions may involve negative connotations, as happened with engineered nanoparticles (NPs), doubtless and unfortunately due to the lack of rigorous analytical and toxicological controls about these nanometric formulations of quercetin (from now referred to as nanoquercetin). It might likely that many of these nanometric particles show adverse effects due to their small size and rapid diffusion throughout the body, specifically above a certain dose, reason why the need for stability studies in food samples and their related analytical and nanotoxicological evaluations becomes of great concern [5]. Therefore, evaluating and quantifying the successful manufacture/addition and stabilization of nanoquercetin in food and complementary matrices turn crucial to ensure consumer safety.

Until now, most investigations have focused on the determination of unencapsulated/free quercetin using different analytical techniques, such as voltammetry [14], mass spectrometry [15], colorimetry [16], fluorimetry [17], spectrophotometry [18], capillary electrophoresis [19], liquid chromatography [20], gas chromatography [21] and Raman spectroscopy [22]. Remarkably, only a few studies reported the detection of encapsulated quercetin mainly using high-performance liquid chromatography (HPLC) [23,24], although its quantification always implied the disruption of quercetin-containing nanosystems. However, the quantification of quercetin in different nanoformulations while maintaining its original chemical and physical distribution is an analytical topic of great importance from a nanometrological point of view. On the other hand, most of research about quercetin-loaded nanocarriers have just been focused on the study of the physicochemical properties of these nanoformulations but not on the development of suitable analytical methods allowing their quantification in new-design commercial samples containing this encapsulated bioactive.

Attending to the mentioned reasons, among the aims of this research was the establishment of an analytical method that allows quantifying nanoquercetin by preserving its original state inside the chosen formulation. Thus, the first stage involves the synthesis of a food grade nanoemulsion of quercetin by means of a careful selection of the suitable composition (nature and percentage mass/mass), attending to results about encapsulation efficiency (EE), diameter droplet size and polydispersity index and indeed, following GRAS criteria. The low energy method PIT (Phase Inversion Temperature) was the choice to carry out the synthesis procedure [8]. Secondly, the surface-enhanced Raman scattering (SERS) methodology in liquid phase has been used to quantify the synthetized nanoquercetin without disruption of nanoemulsions. To achieve this challenge, metallic anisotropic NPs, such as gold nanorods (GNRs), have been selected as analytical nanotools. GNRs display potential features: high quality synthesis capacity using seed growth [25], superiority in structural self-assembly, light and harvesting ability, flexibility to easily tune their surface plasmon resonance (SPR) band by varying its aspect ratio (AR, ratio of length and width), from the visible to infrared spectrum to match the laser wavelength of portable Raman devices, and in addition, they are biocompatible NPs. GNRs exhibit two surface plasmons, a weak one around 520 nm ($\pm$ 10 nm) corresponding to the transverse SPR and a strong one from the longitudinal SPR whose wavelength can be adjusted between 650 and 1300 nm [25]. All these properties made them excellent candidates for creating new SERS platforms like those 3D liquid-state interfacial plasmonic ones, which exhibit a substantial progress in dealing the lack of reproducibility affecting conventional solid substrates in SERS analysis inherent to the irregular hotspots distribution, since the designed 3D system provides an improved homogeneous distribution of NPs and of their subsequent SPR couplings generating in this way a regular hotspots distribution [26].

Herein, an innovative analytical methodology was developed, focusing on four main purposes. The first one aims at discriminating between free and encapsulated quercetin (Q-NEs), which would involve a second goal, i.e., the synthesis and properly characterization of stable Q-NE nanoformulation. The third goal corresponds to the development of a liquid-state SERS methodology, and the fourth one, to quantify Q-NEs keeping their native nanostructures. All research developed herein is encompassed within the analytical nanometrology through the third way, incorporating simultaneously nanomaterials as both tools and analytes. Finally, applicability of the nanometrological procedure was tested on native commercial dietary supplements and validated using reversed-phase micro-high-performance liquid chromatography-diode-array detection (RP-μHPLC-DAD) with consistent results.

2. Materials and methods

2.1. Reagents and solutions

All the used reagents were "analytical grade" quality. Castor oil, polyethylene glycol sorbitan monooleate (Tween 80), quercetin (≥95%), Saponin Quillaja sp. Sapogenin content 30–35%, sodium hydroxide (98%), ethanol (99%), hydrogen tetrachloroaurate trihydrate ($HAuCl_4 \cdot 3H_2O$, ≥99.9%), silver nitrate ($AgNO_3$, ≥99.0%, ACS reagent), sodium borohydride ($NaBH_4$, 99%), L-Ascorbic acid (vitamin C, ≥99.0%), hexadecyltrimethylammonium bromide (CTAB, H9151, ≥99%), poly(sodium 4-styrenesulfonate) solution (Na-PSS, 30 wt% in H_2O), hydrochloric acid (HCl, 37%, Merck), acetonitrile (≥99.9%), glacial acetic acid (≥99%), magnesium stearate (technical grade), microcrystalline cellulose, titanium oxide (TiO_2, ≥99%), sodium chloride (NaCl, ≥99.0%, ACS reagent), copper chloride ($CuCl_2$, 97%), magnesium sulfate ($MgSO_4 \cdot 7H_2O$, ≥98%, ACS reagent), cholecalciferol (≥98%), tocopherol (vitamin E, ≥95.5%), riboflavin (98%), pyridoxine (≥98%), calcium chloride ($CaCl_2$, ≥93.0%) and 2-(N-morpholino) ethanesulfonic acid (MES hydrate, ≥99.5%) were acquired from Sigma-Aldrich (St. Louis, USA, www.sigmaaldrich.com/spain.html).

Commercial dietary supplements containing nanoencapsulated quercetin were acquired from the international market (One Planet Nutrition and ActiNovo). The functional drink Vitamin Well Antioxidant was obtained through local distributors. All these products belong to recognized brands and their declared composition was:

Nano Quercetin, capsules (One Planet Nutrition, EE.UU.): Aqueous Nano Quercetin, Vegetable Capsule, Rice Flour. It does not contain soy, corn, yeast, wheat, gluten, milk, egg, fish, shellfish.

Liposomal Quercetin, liquid (Actinovo, Germany): Purified water, phospholipids, acid, and natural sea buckthorn extract.

Vitamin Well Antioxidant (Sweden): source water, fructose, acidity correctors (citric acid, sodium citrate), green tea extract, elderberries extract, grape shell extract, pomegranate extract, vitamins (E, C), minerals (zinc, manganese, selenium), peach aroma, green tea extract may appear as small particles in drink.

All solutions were prepared using ultrapure water 18.2 MΩ cm (25 ºC) obtained with a Milli-Q system (Millipore, Bedford, MA, USA) and the analytical grade reagents before listed.

2.2. Instrumentation

An ultrasound bath (Selecta, Barcelona, Spain), a BioSan high-speed mini-centrifuge Microspin 12 (LabNet Biotecnica S.L., Spain) and a pH-meter (Crison Instruments S.A., Spain) were used at different experimental stages. Absorption spectra of Q-NEs, quercetin and AuNPs solutions were achieved with a SECOMAM UVI Light XS 2 spectrophotometer equipped with a LabPower V3 50 using 10-mm quartz cuvettes. Particle size distribution, polydispersity index and zeta potential of Q-NEs were determined by dynamic light scattering (DLS) measurements using a Zetasizer Nano Series DLS ZEN3500 (Malvern Instruments Limited, Spain). Raman and SERS experiments were conducted on a portable BWTek i-Raman (Model # BWS465-785S) equipped with a standard BCR100A accessory for liquid phase

measuring in a common cuvette. This equipment included a laser wavelength of 785 nm and maximum output laser power of 348 mW at the excitation port and 285 mW. An Agilent Technologies HPLC system (series 1200, Waldbronn, Germany) was utilized for the chromatographic analysis, which were performed on an Zorbax SB-C18 column (5 μm particle size ODS, 150 x 0.5 mm) from Agilent. This system consists of a solvent reservoir, degasser, a pump, an autosampler, thermostatted column compartment and a 1260 Infinity model diode-array detector. Scanning electron microscopy (SEM) images were taken with a ZEISS GeminiSEM 500 microscope to evaluate shape, size, and morphology for AuNPs and Q-NEs. Real-time imaging of Q-NEs in solution were performed in a ZEISS fluorescence confocal microscope (Vert.A1-Axiocam 702 mono) in the absence and presence of light. This microscope is equipped with a fluorescence laser with emission filter centered at 530 nm and two objective lenses from 10x to 40x for magnification. The solution containing the organic nanoparticle was inserted in a microfluidic channel and the nanosized emulsion was recorded with and without irradiation.

2.3. Synthesis of quercetin-loaded nanoemulsions

Q-NEs were produced using the PIT method [8] with some modifications. This process allows making lipid droplets of nanometric size controlling the temperature; in our case these lipid droplets were arranged as o/w nanoemulsions. Briefly, two steps were necessary for this purpose: firstly, mixing and heating and, secondly, cooling, as depicted in **Fig. S1** of **Supplementary Material (SM)** file.

A common detailed PIT procedure consisted of the constant magnetic stirring (460 rpm) for mixing all selected components in their optimized proportion (% w/w): 5.25% castor oil, 0.25% quercetin, 0.55% EtOH, 4.5% Tween 80, 0.5% Quillaja Saponin and aqueous phase up to 100% (ultrapure water at pH values between 5.5 and 6.0 by NaOH addition), with simultaneous rising from room temperature up to 80 °C in a thermostatic bath. Once 80 °C was reached, the formulation remained stirred at this temperature for 20 min to stabilize. Subsequently, it was quickly cooled to 10 °C by immersing the beaker in ice water while the magnetic stirring continued at 460 rpm. Once 10 °C had been attained it was kept stirring for 20 min for stabilization. Both cycles of heating and cooling were repeated two more times.

After synthesis, the final formulation was centrifugated for 40 min at 5000 rpm with the aim of separating the free quercetin and Q-NEs. Finally, the free quercetin precipitated at the bottom of the Eppendorf and Q-NEs (supernatants) were extracted with a syringe.

2.4. Synthesis of diverse gold nanoparticles

The AuNPs with spherical, square and rod like shapes were synthesized by a classical method based on seed growth previously described [27]. The preparation of the seeds was carried out without modifications. However, some variations were made in the synthesis of GNR which are described as follows: 0.03 mL of 0.01 M $AgNO_3$ solution were added with mild stirring on 4.75 mL of 0.1 M CTAB. Agitation was continued for 5 min and then it was kept standing for 15 min in a thermostatic bath at 30 °C. Then, 0.2 mL of 0.01 M $HAuCl_4$ solution was added, and it was left to stand for 5 min. Afterwards, 0.032 mL of freshly prepared 0.10 M ascorbic acid were quickly added to the above solution vigorously stirred. After 1 min of stirring, the solution was kept standing again for 30 min in a thermostatic bath at 30 °C. Finally, 0.010 mL of seeds were added to this last solution, and then this mixture was let to stand still between 8 and 12 h in a thermostatic bath at 30 °C.

Once synthesized, GNRs were subjected to a ligand exchange procedure to replace CTAB by citrate by means of a protocol based on five sequential cycles of centrifugation and redispersion [28]. The first cycle was related to the purification of the GNR solution. To achieve it, the solution was centrifuged for 15 min at 13,500 rpm to remove most of CTAB by bringing out the 95% of the supernatant phase and subsequently reconstitution with MilliQ water. Then, two additional cycles of centrifugation/redispersion (under the same conditions) were carried out, keeping the solution at rest for 1 h between each cycle. In these cycles the nanorods solution was redispersed in 0.15% Na-PSS (w/w); in this step, gold nanobones (Bn) were already formed. This solution was later centrifuged under the same conditions and redispersed using 5 mM sodium citrate and kept at rest for 12 h to replace Na-PSS by citrate. Finally, a fifth cycle of centrifugation / redispersion was carried out in 5 mM of sodium citrate. Concentrations of AuNP solutions were denoted as OD (optical densities).

The procedure for the synthesis of cubic [29] and spherical [30] nanoparticles was like that of nanorods but with different aliquots for the involved reagents. The volumes and concentrations used in both the seed and growth processes are shown in **Table S1** of **SM** file.

2.5. Sample treatments

The experimental procedure for the analysis of dietary supplements with claimed nanoquercetin-containing were as follows:

For Nanoquercetin samples from One Planet Nutrition, the content corresponding to a capsule (0.5 g) was dissolved in 250 mL MilliQ water and stirred for 15 min, whereas for the Actinovo commercial solution, a 1:100 dilution was prepared in MilliQ water. After that, for both samples, an aliquot (2 mL) was taken to an Eppendorf and centrifuged for 30 min at 5000 rpm to remove non-encapsulated quercetin and aggregates. Then, the supernatant was transferred to another Eppendorf. At this stage, the size of encapsulated nanoquercetin droplets was determined by DLS whereas the quercetin content inside the nanoemulsions was quantified using the developed liquid state SERS method.

Alternatively, the functional drink *Vitamin Well Antioxidant* was spiked at three concentration levels between 5.6 and 22.5 μM of Q-NEs.

All SERS analyses were performed by mixing a suitable GNRs volume (to get 0.6 OD as final concentration) and the supernatant phase from centrifuged samples to reach a final volume of 2 mL, which was stirred for 5 min at 200 rpm in the darkness and transferred to a quartz cuvette for the liquid SERS measurements.

2.6. SERS procedure

SERS experiments were performed with a laser excitation wavelength of 785 nm, an exposure time of 40 s, one accumulation scan and a 40% output laser power in the probe. SERS measurements were carried out at room temperature on 2 mL solutions containing 0.55 mL of 2.19 OD GNRs and different Q-NEs concentrations from the supernatant phase reached after centrifugation process. These solutions were stirred with a magnetic microbead for five min in the dark. Finally, they were transferred to the cuvette and inserted into the Raman accessory.

Information regarding "**Characterization of quercetin-loaded nanoemulsions**", "**Characterization of plasmonic nanomaterials**" and "**RP-μHPLC procedure"** sections are given as **S1-S3** sections in **SM** file.

3. Results and discussion

3.1. Optimization of Q-NEs synthesis

Regarding quercetin encapsulation into delivery systems such as food grade nanoemulsions where all its components are within the GRAS category, the PIT method was selected for its synthesis. This is a low energy method with superior performance compared to others like spontaneous emulsion and phase inversion composition [31]. The selection of the appropriate components as well as their suitable percentage were selected based on the NPs size, the polydispersity index (PdI) and the entrapment efficiency (EE) of the Q-NEs obtained for this optimization procedure. The whole synthesis optimization process is detailed thoroughly in the section **S4** of **SM**. Table 1 summarizes the

Table 1
Optimization for Q-NEs components (w/w percentage) along PIT synthesis procedure.

Composition	Percentage	Size (Day 1)	PdI
Tween 80	10	247.4	0.255
	5	41.7	0.215
	2	193	0.465
Quillaja Saponin (with aqueous phase water at pH 6)	2	43	0.412
	1.5	57.3	0.549
	1	51.6	0.244
	0.5	64	0.137
Castor oil	15	6.25	0.500
	10	53.2	0.188
	5.25	47.1	0.185
Ethanol	2	6.1	0.462
	1	51.4	0.199
	0.55	53.2	0.188
Quercetin	0.25	53.2	0.188
	0.18	5.7	0.448
	0.15	6.0	1.000
	0.13	5.8	0.597

results for all experiments carried out along the optimization of this synthetic procedure. The optimal percentages (% w/w) for Q-NEs components were 4.5% tween 80, 0.5% quillaja saponin, 5.25% castor oil, 0.55% ethanol and 0.25% quercetin. After carrying out a reproducibility study (n = 6) of this optimized synthesis procedure, the results in terms of droplet size 73.1 ± 2.4 nm, PdI 0.138 ± 0.01 and EE (%) 96.5 ± 1.3 can be considered very valuable data keeping in mind that the PIT process is a low energy method, not submitted to specific and automated instrumentation. The so-synthetized Q-NEs exhibit a concentration of $3.7{\cdot}10^{-3}$ ± 0.0002 M.

All description about nanostructural characterization of Q-NEs appear in **S5** of **SM**.

3.2. Characterization of gold nanoparticles

The GNRs covered with hexadecyltrimethylammonium bromide (CTAB-GNR) were subjected to a ligand substitution process, in which CTAB was exchanged for citrate using the Na-PSS polymer as mediation agent. Citrate-GNR provides a cleaner SPR band with much more long-term stability for low ionic strength dispersions [28]. It is important to highlight that during this ligand exchange process an alteration in the GNRs morphology takes place, changing from rod-shaped to finally bone-like nanostructure (see Fig. 1**A**). This morphological modification

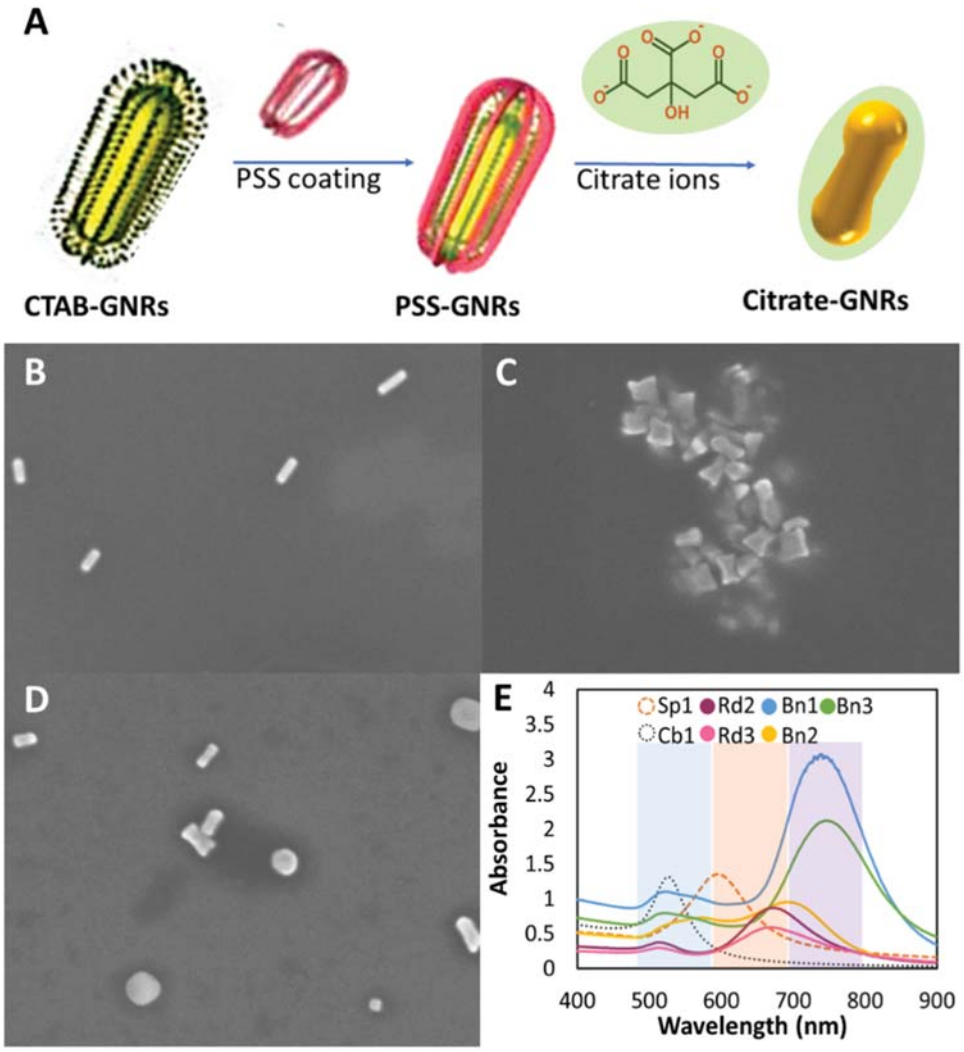

Fig. 1. A) Scheme of the ligand exchange process of CTAB-GNRs via electrostatic self-assembly of PSS and citrate ions leading to the formation of bone-like rods. SEM micrographs of gold nanorods (GNRs) during the surface ligand exchange: B) CTAB-GNR; C) PSS-GNR and D) Citrate-GNR. E) UV-Vis spectra of several gold nanoparticles (AuNPs) with diverse sizes and shapes.

of the GNRs does not affect their SPR absorbance band. The SEM images (Fig. 1**B, C** and **D**) showed this transformation in the morphology of the GNRs along the ligand exchange process. In addition, Fig. 1**E** shows the UV-Vis spectra for all NPs used in this research. In the case of GNRs, because of their shape, two plasmonic bands can be observed due to their cylindrical symmetry. The first band corresponding to the transversal section appearing at around 520 nm (± 10 nm) while the second band corresponding to the longitudinal section can be tuned between 650 and 1300 nm, doing match it to the laser excitation wavelength to reach the SERS enhancement of Raman signal. For AuNPs with spherical (Sp) and cubic shape (Cb), it is typical just observe one plasmonic band close to 540 nm (± 10 nm) as evidenced in Fig. 1**E** for Sp1 (dashed line, spheres) and Cb1 (dotted line, shaped like cubes). Regarding dimensions, all the synthesized NPs were studied by SEM whereas the spherical ones were just characterized by DLS. The results obtained in terms of SPR bands (λ), physical and hydrodynamic sizes, aspect ratios and concentrations denoted as optical densities (OD) for all the synthetized NPs are summarized in Table 2.

3.3. Design of 3D liquid state interfacial SERS system

Liquid state interfacial plasmonic systems are emerging as a smart substrates alternative for a reliable quantification and easier practicability in complex analytical applications, such as the Q-NEs (O/W droplets) as analytes. Experiments on Q-NEs were carried out to study the effect of some specific parameters relative to the different AuNPs plasmonic dispersions which directly influence the EM (electromagnetic) SERS enhancement. It is important to note that, in the liquid state, the NPs, regardless of their morphology, are randomly oriented, therefore, the collected SERS spectra are representative of all possible orientations averaged throughout the acquisition time [32]. However, previous research predicted that GNRs may interact with Q-NEs through their ends, since during the synthesis the surfactant molecules tend to position themselves at the central part of the GNRs, displacing more gold atoms towards the ends, and exhibiting therefore a greater interaction by these endings [26]. The optimal conditions were selected based on the improvement in signal intensity, i.e., the analytical enhancement factor (AEF):

$$AEF = \frac{I_{SERS}/C_{SERS}}{I_{RAMAN}/C_{RAMAN}} \quad (1)$$

Where I_{SERS} y I_{RAMAN} correspond to the SERS and Raman intensities respectively, while C_{SERS} y C_{RAMAN} are related to the concentration of Q-NEs used in SERS and Raman experiments.

For Q-NEs Raman spectra, the sensitive (intense) band at 1600 cm^{-1}, assigned to the stretching mode (C═O), was selected as suitable analytical signal for AEF calculations considering firstly, the magnification effect here exhibited and secondly, its proven linear behavior regarding the analyte concentrations. In this sense, the following parameters should be examined on 55 μM of Q-NEs: different NP coatings of CTAB, Na-PSS and citrate; location of the displayed SPR bands in the range from 527 to 989 nm (Fig. 1**E**); different morphologies (spherical, nanocubes and nanorods) (Fig. 2**A** and 2**B**), different sizes (Fig. 2**C**) and optimal concentrations of the selected NPs (Fig. 3**A**).

The first step was to study what type of ligand (CTAB, Na-PSS and citrate) favored the EM intensity improvement for the subsequent quantification of Q-NEs. After conducting several experiments, it was observed that CTAB-GNRs yielded the worst results, possibly due to an increase in steric impediment which difficult the orientation of Q-NEs towards the surface of GNRs [26]. In contrast, charged citrate anions chemisorbed onto the surface of AuNPs (bone shaped) which enable the approaching of the gold atoms at optimal distance from quercetin inside the nanoemulsion system showing thus the best results in terms of signal magnification (**Fig. S4**). This improvement in the signal is mainly attributed to changes in AuNP morphology during the ligand exchange process of GNRs (Fig. 1**A**), with evolution from cylindrical to a bone-like shape after the uneven coating of CTAB and subsequent Na-PSS and citrate steps that induces atomic rearrangements of AuNPs [26].

Once the citrate coating was selected, these citrate-AuNPs were synthesized attending to different morphologies (spherical, nanorods and cubes). Since the equipment laser excitation wavelength was 785 nm, a near and wide range of SPR bands was tested for the so-synthetized AuNPs, that was: < 600 nm, 600–700 nm, 700–800 nm and > 800 nm. As shown in Fig. 2**A**, preliminary experiments showed that GNPs denoted as Rd1 (SPR 989 nm), Sp1 (SPR 543 nm) and Cb1 (SPR 523 nm) gave very low enhancement factors as expected since their SPRs bands were furthest from the laser wavelength, as Fig. 2**B** evidences. On the contrary, those GNRs with longitudinal plasmon appearing between 650 and 750 nm showed an improvement of the Raman signal and specifically the Bn1 presented the best AEF in these initial proofs. Then, these preliminary results allowed to rule out the use of NPs with spherical (Sp1) and cubic morphologies (Cb1) as plasmonic enhancers, evidencing greater factors for nanorods as displaying two directions along to polarize the incident light (Fig. 2**A** and **B**). The AEF differences between GNRs with a SPR band in the range from 650 to 750 nm can be mainly attributed to three factors: aspect ratio value, resonance with the Q-NEs absorption band (375 nm) and sizes. Thus, it was observed that GNRs with very high or small aspect ratios showed AEFs significantly lower than that of Bn1 (Fig. 2**C),** where the following sequence is evidenced: 3.2 (Rd3) > 2.6 (Rd2) > 2.2 (Bn1) > 2.1 (Bn3) > 1.2 (Bn2). Special mention must be done for the Bn3 (SPR 746 nm), which presented similar aspect ratio to Bn1 and a SPR band closer to the laser frequency, so they should be theoretically more resonant, but however, it showed worse performance than that Bn1. The suitability of Bn1 versus Bn3 can be explained attending to its shorter plasmon band (719 versus 746 nm) better fitted to be resonant with the quercetin absorption band (376 nm). Besides, the influence of their different sizes should be considered, since upon findings of previous research [33,34], too large or small GNPs become less resonant, displaying worse resolution and more noise than those with an intermediate size such as 60–70 nm (Table 3). In addition to these considerations regarding AEF values, the selected nanorods-bone shaped displayed an excellent resolution on the characteristic bands of Q-NEs compared to the rest of tested AuNPs (Fig. 2**D**).

Next step was focused on selecting the optimal concentration of the already selected plasmonic nanomaterial (Bn1) to obtain the maximal AEF. GNB concentration was evaluated in the range 0.5–3 OD, reaching the best results for 0.6 OD (Fig. 3**A**). It must be stand out that this value is significantly lower than other reported in consulted bibliography [26].

Once optimized all influencing variables, the final AEFs were $1.2{\cdot}10^3$ and 1.0 10^5 upon the *Eq. A*, for the Q-NEs (stretching at 1600 cm^{-1}) and for a suitable Raman reporter such methylene blue (stretching at 446 cm^{-1}), respectively (Fig. 4**A and B**).

It is important to emphasize that AEFs obtained using solid conventional SERS substrates are currently higher than those resulting from new smart substrates, e.g., 3D liquid state SERS, flexible, dynamic SERS

Table 2
Stability study about hydrodynamic diameter, polydispersity index and concentrations of Q-NEs along 30 days period.

Parameters	Day 1	Day 4	Day 7	Day 10	Day 15	Day 20	Day 30
Size (nm)	78.7 ± 1.5	76.8 ± 0.4	78 ± 0.5	77 ± 2.3	76.3 ± 2.7	80.9 ± 1.4	86.1 ± 3.3
PdI	0.171 ± 0.005	0.189 ± 0.010	0.185 ± 0.001	0.197 ± 0.004	0.193 ± 0.013	0.160 ± 0.007	0.155 ± 0.007
Concentration (M)	$2.1{\cdot}10^{-3} \pm 1.7{\cdot}10^{-5}$	$1.8{\cdot}10^{-3} \pm 2.3{\cdot}10^{-5}$	$1.5{\cdot}10^{-3} \pm 1.6{\cdot}10^{-5}$	$1.3{\cdot}10^{-3} \pm 1.8{\cdot}10^{-5}$	$1{\cdot}10^{-3} \pm 3.1{\cdot}10^{-6}$	$9{\cdot}10^{-4} \pm 3.8{\cdot}10^{-6}$	$1.6{\cdot}10^{-4} \pm 3.8{\cdot}10^{-6}$

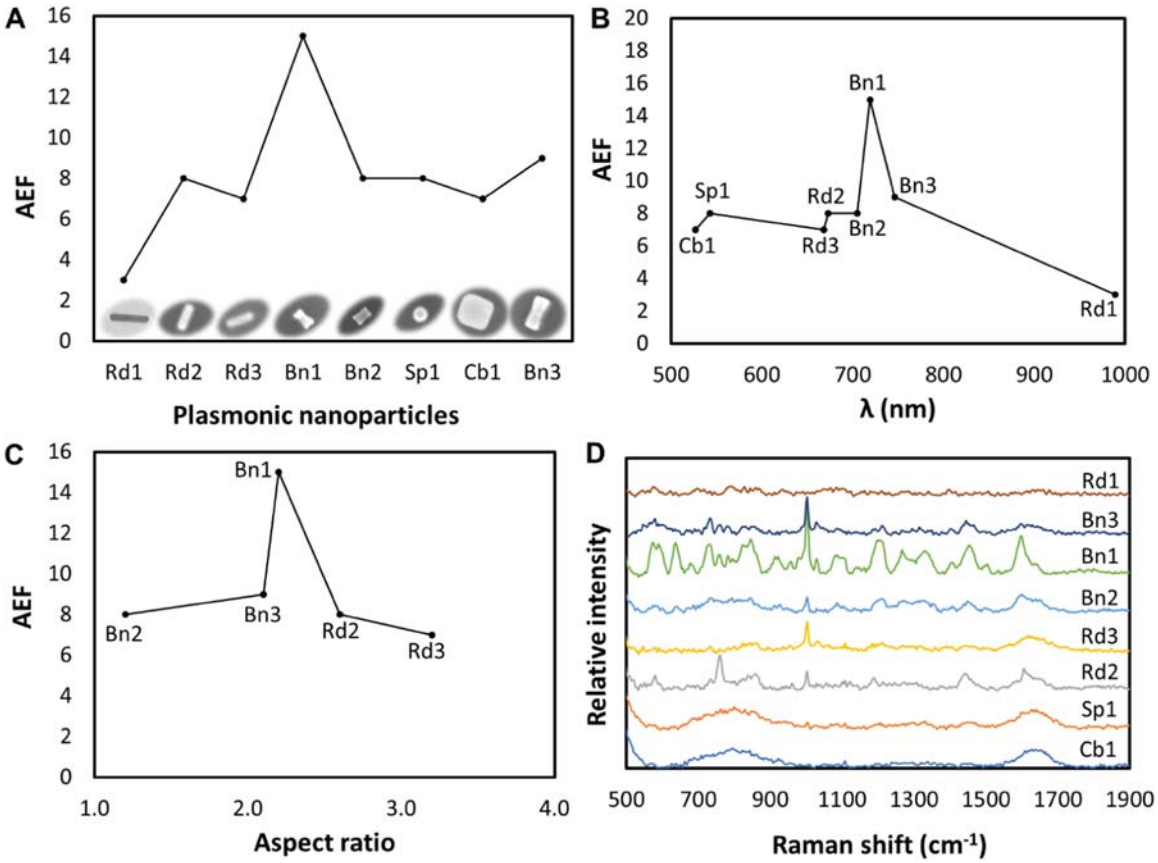

Fig. 2. Obtained EM analytical enhancement factors on the 1600 cm-1 stretching for 55 μM Q-NEs considering: A) different AuNPs at 0.8 OD, B) attending their SPR band location, C) aspect ratio values and D) enhanced Q-NEs Raman spectra using different + 0.8 OD nanoparticles: Cb1 (1), Sp1 (2), Rd2 (3), Rd3 (4), Bn2 (5), Bn1 (6), Bn3 (7) and Rd1 (8).

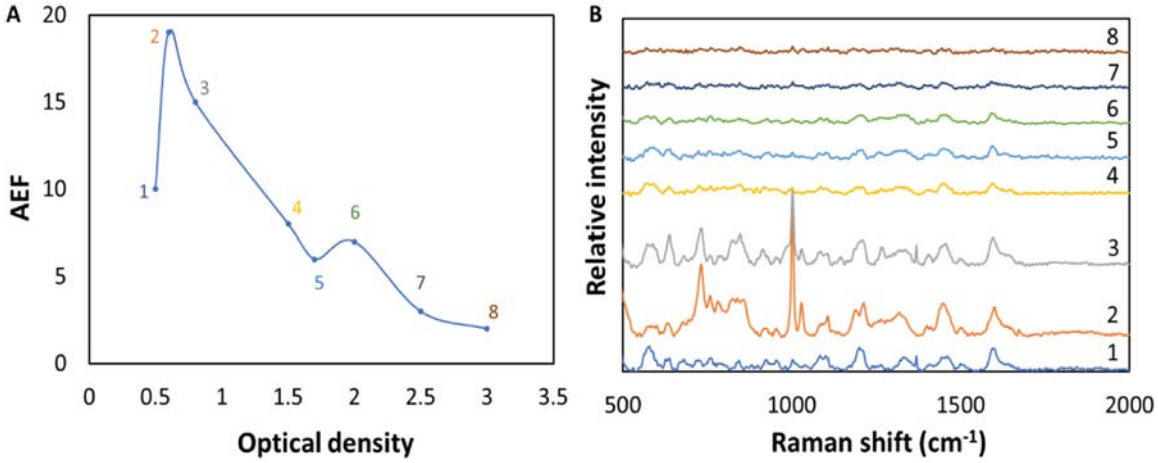

Fig. 3. A) Selection of plasmonic NPs (Bn1) concentrations denoted as OD units. B) Stacked SERS spectra for 5.5·10–5 M Q-NEs obtained at OD values reflected in A) (from 0.5 to 3.0).

[35], etc. These are recently emerging methodologies, which are nowadays in development process and can represent a great advance for those analytical applications addressing complex samples such as lipidic organic nanomaterials (nanoemulsions, nanoliposomes, micelles, solid lipid nanocarriers and NP lipid carriers). In fact, in other published works using this 3D methodology, the target analytes were not nano-sized while in this work complex systems such as Q-NEs are determined without altering their native nanostructure.

Besides these systems involve a marked improvement of the main challenge affecting SERS analysis, that is the lack of reproducibility inherent to the irregular hotspots distribution in solid substrates. In the present research, the PML (plasmonic metal liquid) interface provides a 3D self-assembling plasmonic arrays in the spherical oil-water interfaces (Fig. 5**D**) with a homogeneous distribution of GNBs and of their subsequent SPR couplings generating so regular hotspots distribution. This drives to an increase in observed reproducibility (Section 3.6), even without the need to use internal standard. Furthermore, harmful organic solvents were not necessary to create the 3D interfacial SERS platforms

Table 3
Summary about SEM and hydrodynamic sizes, SPR bands (λ), aspect ratios (AR) and concentrations (OD) for all the synthesized gold nanoparticles: spheres, cubes, bones and nanorods.

Type of nanoparticle	Shape	Length (nm)	Width (nm)	λ_{WIDTH} (nm)	λ_{LENGTH} (nm)	Hydrodynamic size (nm)	$AR_{DIMENSION}$	OD
Rd1	Rod	69.3	12	530	989	–	5.78	1.1
Rd2	Rod	58	22	520	673	–	2.64	1.0
Rd3	Rod	38	12	520	668	–	3.17	50.0
Bn1	Bone	67	31	530	719	–	2.16	2.2
Bn2	Bone	143	121	530	705	–	1.18	1.2
Bn3	Bone	103	49	521	746	–	2.10	2.1
Sp1	Sphere	–	92.5	–	543	85.2	–	2.0
Cb1	Cube	121	112	–	527	–	–	1.3

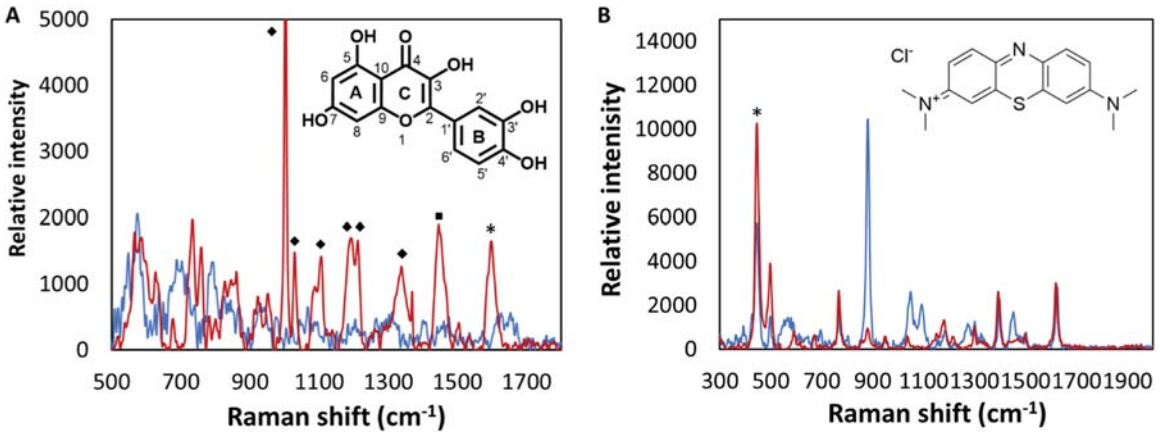

Fig. 4. A) Raman spectrum of $3.2{\cdot}10^{-4}$ M Q-NEs (blue line) and SERS spectrum of 10^{-6} M Q-NEs in presence of GNBs (red line) and B) Raman spectrum of 1 mM (blue line) and SERS spectrum of 1 μM methylene blue in presence of GNBs (red line) in a quartz cuvette.

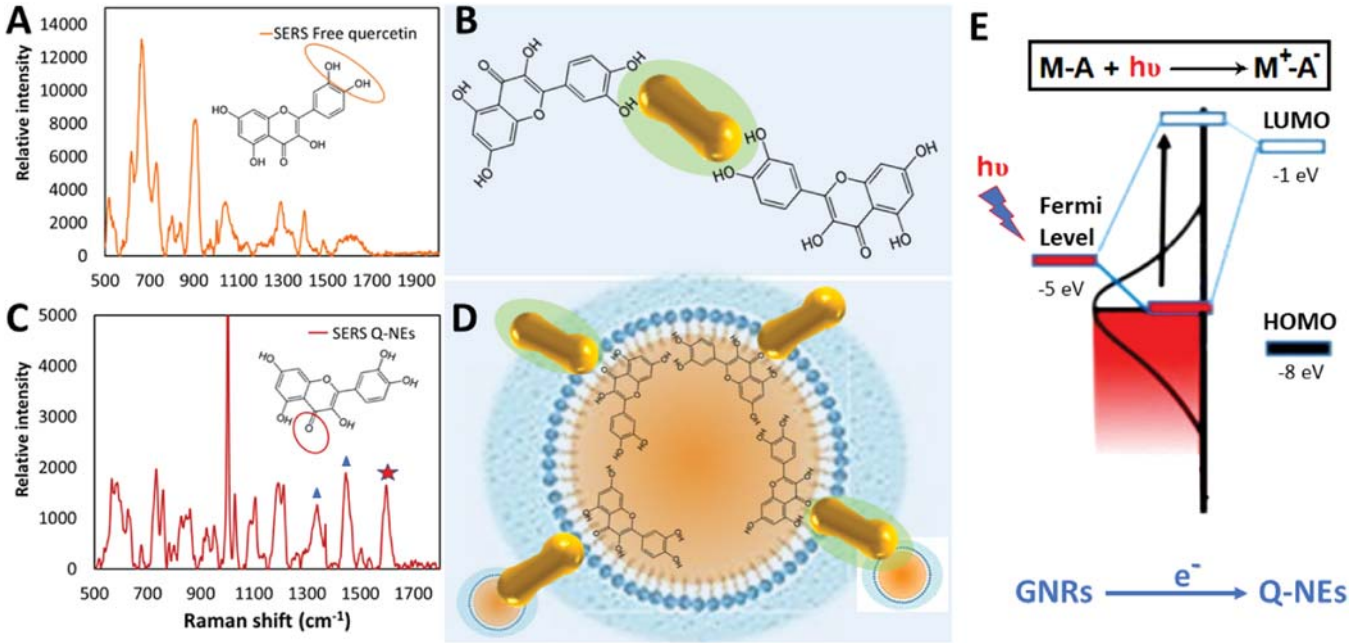

Fig. 5. A) Free quercetin SERs spectrum and B) expected interactions between GNBs and free quercetin; C) Q-NE SERS spectrum and D) proposed interactions between GNBs and encapsulated quercetin as nanoemulsion; E) diagram about the energy levels of metal (left) and quercetin (right) in the nanoemulsion system and transitions involved in the charge transfer mechanism from the metal NPs to the adsorbate.

as described in previous research [26,36], since the organic phase was already supplied by the analyte itself (Q-NEs with Castor oil as GRAS organic phase).

Optimization of instrumental parameters for measuring in the designed PML interface system is described in **S6** of **SM** (**Fig. S5**).

3.4. Discrimination between free quercetin and quercetin-loaded nanoemulsion

Discrimination between free and nanoencapsulated quercetin was accomplished by three strategies: ***A)*** UV-Vis spectrophotometry, ***B)***

Raman spectroscopy, both shown in detail in Section 3.2 (**Fig. S2C and Fig. S3A**, respectively) and ***C)*** SERS: the aforementioned differences are much more pronounced for both analytes in the presence of GNBs. Fig. 4**A** focuses on the typical peaks of the encapsulated quercetin displayed at ca. 575 cm^{-1} and 1600 cm^{-1}. The last region attributed to the carbonyl stretching mode implies transformation when interacting with GNBs. Thus, the three bands for Q-NE appearing at 1574, 1616 and 1625 cm^{-1} in the absence of GNBs (**Fig. S3A**) are switched into a single band at 1600 cm^{-1} (*) in the presence of GNBs. Furthermore, a significant peak was observed at 1446 cm^{-1} (Fig. 4**A**, ■) in the presence of GNBs which was attributed to three of the emulsion components, namely castor oil, ethanol, and tween 80 (**Fig. S3B**). The remaining peaks appearing at 1330, 1210, 1195, 1104, 1086, 1028, 1002 cm^{-1} (Fig. 4**A,** ◆) also correspond to components of nanoemulsion, except for quillaja saponin which does not exhibit any characteristic Raman band. These peaks have a similar morphology to that of the separated components displayed in **Fig. S3B**, although their position had undergone slight displacements due to formation of the nanoemulsion (inherent polarizability changes in environment). Then these two facts, that are the convergence of the three peaks (1574, 1616 and 1625 cm^{-1}) in an enhanced single one centered at 1600 cm^{-1} and the displacements of the rest of them, may indicate that the interaction between GNBs and the Q-NEs takes place through the two SERS mechanisms which are described in the following section [32].

Remarkably, free quercetin showed a different behavior in the presence of GNBs. For free quercetin, the stretching located at 600 cm^{-1} was enhanced (assigned to the bending out of the plane of the C-C skeleton from the A and C rings) whereas the magnification occurs at 1600 cm^{-1} for encapsulated quercetin (Fig. 5). It would involve a distinctive steric orientation and, consequently, different interactions between quercetin and GNBs in these two different situations.

3.5. SERS mechanism

Regarding the possible enhancement mechanisms involved, EM effects may occur because of the specially fitted SPR band of GNBs matching the laser' excitation wavelength (Section 3.3), as well as by a chemical mechanism or charge transfer process (CT) for which quercetin is also especially suited due to its conjugated systems and sensitive oxygen-containing groups, namely catechol part OH(3`)/OH(4`), and those from condensate rings via OH(3)/OH(4) and C═O(4)/OH(5) groups.

Considering the enhanced stretching of free quercetin in the presence of GNBs (600 cm^{-1}**,** Fig. 5**A**), we proposed a CT mechanism where a complex M-A (metal-adsorbate) is established via a chemisorption process through the "first layer effect" [37]. A non-radiative CT mechanism is then involved usually by means of chemisorption thought non-bonding doublet electrons of diverse heteroatoms (OH groups of catechol ring, Fig. 5**B**) on metallic surface [38]. This binding orientation of quercetin is also proved by the enhancement and shifting displayed by the OH vibrational modes of the catechol ring, which should be sheer located towards the GNBs (Fig. 5**A and B**) and their irradiated electromagnetic field, according to EM mechanism selection rules. However, lack of variation in the stretching modes of C(4)=O and C(2)=C(3) (ca. 1460–1660 cm^{-1}) suggests that they were not involved in the interaction with GNBs.

According to the selective intensification displayed for Q-NEs (Fig. 5**C**), the interaction between encapsulated quercetin and GNBs occurs through the carbonyl group (a downward strong peak in presence of gold atoms at 1600 cm^{-1}) and the hydroxyl group (C(3)-OH, strong band at ca. 1341 cm^{-1}) just adjacent to this carbonyl, together with the OH groups at the C(5) and C(7) of the A ring (very intense band at ca. 1446 cm^{-1}) upon available bibliography [39]. However, as detailed in the previous section, both stretchings also overlap with those of other components of Q-NEs, thus, the stretching at 1600 cm^{-1} corresponding to carbonyl vibration mode was chosen as single analytical signal. In this interfacial nanosystem, the big change in the carbonyl stretching mode in contact with GNBs (enhanced quercetin stretching) suggests a chemisorption process through C(4)=O group, whose vibrational modes perpendicularly located to the metallic surface produced a higher intensification.

It is known that larger AEFs are obtained for distances analyte molecules -metal NPs close to 1–10 nm [40]. In fact, appropriate distances to achieve higher SERS intensifications were reached when quercetin is encapsulated attending to the already described sizes for GNBs (67 x 31 nm) and for Q-NEs droplets (73.1 ± 2.4 nm). Thus, they form a 3D interfacial SERS system in which GNBs are located between the polar heads of surfactant molecules but oriented along the hydrophobic tails towards the encapsulated quercetin (Fig. 5**D**). Regarding the SERS chemical mechanism here posed, the CT process occurs from the Fermi level of GNBs to the lowest unoccupied molecular orbital (LUMO) [39], as depicted in Fig. 5**E**. Thus, quercetin in the nanoemulsion (right) is rearranged directing its carbonyl group of the condensate ring towards the metal NPs favouring the CT process for the metal-adsorbate system (Fig. 5**D**).

3.6. Analytical figures of merit

The analytical performance characteristics of the proposed 3D interfacial SERS methodology were evaluated for the selected analytical signal based on the stretching at 1600 cm^{-1} of Q-NEs to evidence its suitability for quantitative analysis. The obtained analytical features are summarized in Table 4. Precision was evaluated by means of repeatability and reproducibility studies. The repeatability of the proposed SERS method was carried out with fifteen independent measurements at 7.5 μM Q-NEs (with 0.6 OD GNBs) solutions obtaining a relative standard deviation of 2.6%. On the other hand, reproducibility was checked for different Q-NEs solutions in three consecutive days (n = 15 3), with an RSD = 3.6%. These results evidenced the very good precision reached for the developed liquid interfacial method considering that both GNBs and QNEs are not synthesized in an automated way. The designed approach implies great advances in one of the main challenges of SERS techniques, the lack of reproducibility.

The linear dynamic range was established between 0.5 and 30 μM with the linear regression fit displayed in Table 4 and where each concentration level was analyzed in triplicate by means of 0.6 OD GNBs as plasmonic tool (Fig. 6). LOD and LOQ were 0.2 and 0.5 μM, respectively. LOQ was empirically established as the lowest Q-NES concentration able to be quantified by the developed methodology, and it was consistently assigned to the first point of the calibration range. Then, according to IUPAC criteria, LOD was defined as LOQ/3.33 [41].

An exhaustive interferences study was performed with the aim to assess the selectivity of the developed analytical methodology. The effects of different compounds usually present in the analyzed dietary supplements formulations, such as diverse vitamins (vit C, E, D, B_2 and B_6) and electrolytes (Na^+, Ca^{2+}, Cu^{2+}, Mg^{2+}, K^+, Cl^-, SO_4^{2-}) were checked on a solution containing 15.0 μM Q-NEs (with 0.6 OD GNBs again) in different ranges: 0:1, 0.5:1, 1:1, 2:1. The results of these

Table 4
Analytical performance characteristics.

Analytical feature	Q-NEs (μM)
Linear dynamic range	0.5 – 30
Calibration graph	
Intercept	773.29 ± 8.78
Slope (μM^{-1})	29.978 ± 6.44·10^{-1}
Correlation coefficient	0.997
Detection limit	0.2
Quantification limit	0.5
Repeatability RSD(%)* (n = 15)	2.6
Reproducibility RSD(%)* (n = 3)	3.6

* 7.5 μM Q-NEs.

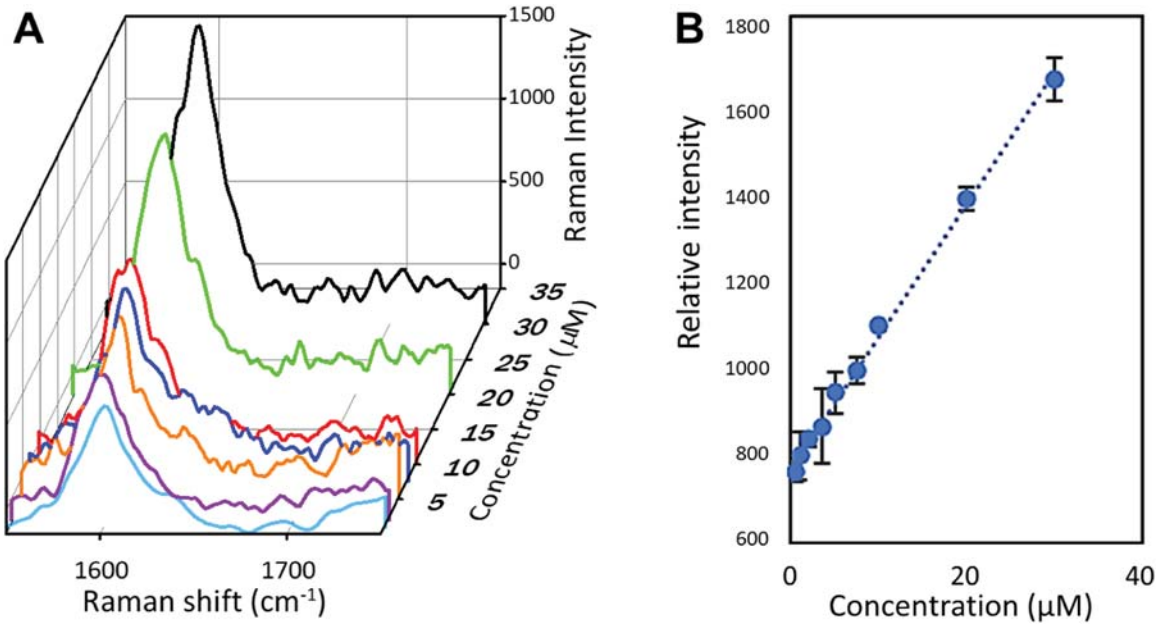

Fig. 6. A) SERS spectra corresponding to concentrations of Q-NE between 0.5 and 30 μM. B) Linear relationship of the enhanced Raman Intensity (1600 cm^{-1}) versus concentration of encapsulated quercetin in the nanoemulsion.

performed experiments are displayed in **Fig. S6**, and evidenced their suitability about selectivity proofs, except for those relative to the Cu^{2+} influence over the analytical signal, where it can be seen a magnification of the intensity, which is due to its already know plasmonic properties. On the other hand, other potential interfering compounds also presents in these nutraceutical supplements, such as some stabilizers and anti-caking agents, i.e., magnesium stearate, microcrystalline cellulose, and titanium oxide, are not soluble in aqueous medium, so they were just removed by centrifugation of the samples.

In contrast to other methodologies related to quercetin analysis already reported in bibliography, *e.g.*, Raman [22] (quantify free quercetin), and RP-μHPLC [23] (quantify nano quercetin), the herein pose presents advances in terms of simplicity, low cost, portability, LOQ, reproducibility (without internal standard) and mainly, the measuring of nanosized analytes without altering its native nanostructure.

3.7. Applications to nutraceutical samples

The developed 3D SERS methodology was applied to the analysis of three real samples; two nutraceutical supplements for which their suppliers declared the presence of quercetin encapsulated in nanosized formulations, from One Planet Nutrition and Actinovo companies respectively, and a functional drink Vitamin Well Antioxidant spiked with the synthetized Q-NEs. These commercial samples were firstly prepared and submitted to the experimental procedure already described in Section 2.5.

For the sample from One Planet Nutrition, three methodologies were tried to isolate nanoquercetin droplets, that were, centrifugation and filtration with two types of filters, nylon membrane of 0.45-μm pore size and pleated filters, respectively. It must be emphasized that a high polydispersity degree was observed for the treated samples by means of any of these separation procedures, despite the different tried methodologies. Specifically, relative to the use of the pleated filter, it was achieved the remotion of aggregates and much of the free quercetin but not all of it. The size measurements of the nanoformulation fluctuate then between 297 and 748 nm. With regard the nylon filter, due to the high number of larger particles preventing the small proportion of smaller particles passing through the filter, it was not observed nanosized quercetin. Finally, when the sample was centrifuged, the aggregates, the free quercetin, and the particles with higher size precipitate; the size then obtained was in the range 147–433 nm. Thus, centrifugation was the selected methodology, but as it has been already reported the obtained quercetin fraction never was nanosized for One Planet Nutrition product although they claim otherwise. For Actinovo product, the size found after centrifugation was of 92 ± 0.6 nm.

Next, the amount of nanoquercetin was evaluated by the application of the SERS methodology on supernatant from centrifugations, spiked with 0.6 OD GNBs. As a further validation study and with the aim to prove the reliability of the proposed 3D interfacial SERS strategy, both supernatant fractions were also submitted to RP-μHPLC-DAD analysis (method in section **S3** of **SM**). Here, the quercetin dynamic range was found to be linear from 0.33 μM to 23.2 μM; its linear regression fit was: $y = (333.16 \pm 5.58)\ x - (53.763 \pm 1.94{\cdot}10^{1})$ with a regression coefficient of 0.9986. All the results obtained via SERS and RP-μHPLC-DAD analysis (n = 3) for both nutraceutical samples were reflected in Table 5**.** This table also shows the found recoveries for Q-NEs when the functional drink Vitamin Well Antioxidant was spiked at three concentration levels in triplicate, with good agreement between the amount added and those found in all levels. Besides, through DLS analysis, it was found that Q-NEs size droplets remains unchanged after the addition into this product.

Subsequently, the paired Student test-*t* was performed between these two sets of data (SERS and chromatographic ones), to verify the statistical accordance between results reported by both methodologies. According to the obtained results (Table 5), in all cases t_0 experimental values were lower than the theoretical one ($t_{(\alpha/2;\ n-1)}$); therefore, it can be guaranteed the absence of significant statistical differences between the results obtained by both methodologies at a confidence level of 95%, which would prove the SERS accuracy at that checked confidence level.

4. Conclusions

This research is a clear example of the third way of Analytical Nanoscience and Nanotechnology which implies the use of analytical nanotools in the determination of nanosized analytes. With this aim, it has been successfully accomplished the synthesis of a food grade nanoemulsion of the hydrophobic bioactive, quercetin, by means of an exigent evaluation of the suitable composition (nature and percentage

Table 5
Analysis of Q-NEs in nutraceutical supplements by interfacial SERS and HPLC techniques. Statistical comparison between results from both methodologies ($\alpha = 0.05$, $n = 4$). * $t_{crit}(\alpha = 0.05, 3$ degrees of freedom, 2 tails$) = 3.18$.

Sample	Size (nm)	Added concentration (μM)	Found concentration by RP-μHPLC-DAD*	Found concentration by SERS*	Recovery (%)	RSD (%)		Exp. t Student t_0
						Concentration	Intensity	
Vitamin Well	73	5.6	5.2 ± 0.1	4.7 ± 0.3	83.1 ± 5.6	6.7	1.0	1.76
Antioxidant (μM)		11.3	11.7 ± 0.1	10.9 ± 0.3	96.7 ± 2.9	3.0	0.9	2.7
		22.5	25.3 ± 0.04	17.4 ± 1.8	77.2 ± 8.2	10.6	4.3	1.21
Nanoquercetin (μM)	147–433	–	15.92 ± 0.26	14.61 ± 0.62	–	1.5	4.2	3.03
Actinovo (mM)	92 ± 0.6	–	5.22 ± 0.22	5.06 ± 0.37	–	2.2	1.6	0.24

* Average of 4 measurements ± standard deviation.

mass/mass), attending to results such as high encapsulation efficiency (96.5%), nanometric droplet size (≤ 100 nm stable for at least 30 days) and polydispersity index. Moreover, nanostructural and physicochemical characterization was in depth addressed not only for the final Q-NE, but along all optimization of the PIT synthesis, what can lay the foundation about the establishment of reference nanomaterials as necessary standards in this field.

Otherwise, an innovative 3D interfacial SERS system has been designed, especially well-suited for this analyte, two phases system itself. These PML platforms are emerging as an alternative for the practicability and accurate quantification of SERS in the analytical science, especially for complex liquid-biphasic systems as the here raised since other techniques already used so far do not allow to evaluate them without disrupt their native nanostructure. This methodology also enables to discriminate between free and nanoencapsulated quercetin based on the distinctive AEF stretchings provided by the different charge transfer interactions exhibited by both ones attending to their different orientations toward GNBs. On the other hand, the designed liquid-state platform has involved a great advance relative to the main challenge affecting SERS quantification nowadays, that is the lack of reproducibility. This is because of the PML interface provides 3D self-assembling plasmonic arrays at the spherical oil-water interfaces with a homogeneous distribution of GNBs and their subsequent SPR couplings generating a regular hotspots distribution. Finally, this 3D liquid SERS development shows excellent applicability results, as evidenced the analysis of new-designed commercial samples containing encapsulated bioactives, with validated results by RP-μHPLC.

CRediT authorship contribution statement

Cristina Montes: Formal analysis, Data curation, Methodology, Investigation, Writing – original draft, Writing – review & editing, Visualization. **M. Laura Dotor**: Investigation, Conceptualization, Writting-Review, Experimental synthesis and characterization, Draft version. **María J. Villaseñor**: Investigation, Methodology, Writing – review & editing, Supervision. **Ángel Ríos**: Investigation, Conceptualization, Writing – review & editing, Supervision, Funding acquisition, Project administration.

Declaration of Competing Interest

The authors declare that they have no known competing financial interests or personal relationships that could have appeared to influence the work reported in this paper.

Acknowledgment

This work was supported by the Spanish Ministerio de Ciencia e Innovación, Spain [grant number PID2019-104381GB-I00] and JJCC Castilla-La Mancha [grant number JCCM SBPLY/17/180501/000262]. M. L. S. expresses her gratitude to European Commission and JJCC Castilla-La Mancha for the funding project SBPLY/17/180501/000333 (PRT program).

Appendix A. Supporting information

Supplementary data associated with this article can be found in the online version at doi:10.1016/j.snb.2022.131509.

References

[1] C. de Carli, M. Moraes-Lovison, S.C. Pinho, Production, physicochemical stability of quercetin-loaded nanoemulsions and evaluation of antioxidant activity in spreadable chicken pâtés, LWT Food Sci. Technol. 98 (2018) 154–161, https://doi.org/10.1016/j.lwt.2018.08.037.
[2] R. Pangeni, S.-W. Kang, M. Oak, E.Y. Park, J.W. Park, Oral delivery of quercetin in oil-in-water nanoemulsion: in vitro characterization and in vivo anti-obesity efficacy in mice, J. Funct. Foods 38 (2017) 571–581, https://doi.org/10.1016/j.jff.2017.09.059.
[3] D.J. McClements, Crystals and crystallization in oil-in-water emulsions: implications for emulsion-based delivery systems, Adv. Colloid Interface Sci. 174 (2012) 1–30, https://doi.org/10.1016/j.cis.2012.03.002.
[4] Q. Huang, H. Yu, Q. Ru, Bioavailability and delivery of nutraceuticals using nanotechnology, J. Food Sci. 75 (1) (2010) R50–R57, https://doi.org/10.1111/j.1750-3841.2009.01457.xg.
[5] C. Montes, M.J. Villaseñor, Á. Ríos, Analytical control of nanodelivery lipid-based systems for encapsulation of nutraceuticals: achievements and challenges, Trends Food Sci. Technol. 90 (2019) 47–62, https://doi.org/10.1016/j.tifs.2019.06.001.
[6] X. Chen, L. Zou, W. Liu, D.J. McClements, Potential of excipient emulsions for improving quercetin bioaccessibility and antioxidant activity: an in vitro study, J. Agric. Food Chem. 64 (18) (2016) 3653–3660, https://doi.org/10.1021/acs.jafc.6b01056.
[7] M.F. Dario, C.A. Oliveira, L.R. Cordeiro, C. Rosado, A.M. Inês de Fátima, E. Maçôas, M.S.C. Santos, M.E.M. da Piedade, A.R. Baby, M.V.R. Velasco, Stability and safety of quercetin-loaded cationic nanoemulsion: in vitro and in vivo assessments, Colloids Surf. A Physicochem. Eng. Asp. 506 (2016) 591–599, https://doi.org/10.1016/j.colsurfa.2016.07.010.
[8] M.F. Dario, M.S.C. Santos, A.S. Viana, E.P. Areas, N.A. Bou-Chacra, M.C. Oliveira, M.E.M. da Piedade, A.R. Baby, M.V.R. Velasco, A high loaded cationic nanoemulsion for quercetin delivery obtained by sub-PIT method, Colloids Surf. A Physicochem. Eng. Asp. 489 (2016) 256–264, https://doi.org/10.1016/j.colsurfa.2015.10.031.
[9] M. Frenzel, A. Steffen-Heins, Impact of quercetin and fish oil encapsulation on bilayer membrane and oxidation stability of liposomes, Food Chem. 185 (2015) 48–57, https://doi.org/10.1016/j.foodchem.2015.03.121.
[10] T. Toniazzo, M.S. Peres, A.P. Ramos, S.C. Pinho, Encapsulation of quercetin in liposomes by ethanol injection and physicochemical characterization of dispersions and lyophilized vesicles, Food Biosci. 19 (2017) 17–25, https://doi.org/10.1016/j.fbio.2017.05.003.
[11] C.P.S. Cazado, S.Cd Pinho, Effect of different stress conditions on the stability of quercetin-loaded lipid microparticles produced with babacu (Orbignya speciosa) oil: evaluation of their potential use in food applications, Food Sci. Technol. 36 (1) (2016) 9–17, https://doi.org/10.1590/1678-457X.6769.
[12] H. Pool, S. Mendoza, H. Xiao, D.J. McClements, Encapsulation and release of hydrophobic bioactive components in nanoemulsion-based delivery systems: impact of physical form on quercetin bioaccessibility, Food Funct. 4 (1) (2013) 162–174, https://doi.org/10.1016/j.jff.2017.09.059.
[13] A. Barras, A. Mezzetti, A. Richard, S. Lazzaroni, S. Roux, P. Melnyk, D. Betbeder, N. Monfilliette-Dupont, Formulation and characterization of polyphenol-loaded lipid nanocapsules, Int. J. Pharm. 379 (2) (2009) 270–277, https://doi.org/10.1016/j.ijpharm.2009.05.054.
[14] S. Takahashi, H. Muguruma, N. Osakabe, H. Inoue, T. Ohsawa, Electrochemical determination with a long-length carbon nanotube electrode of quercetin glucosides in onion, apple peel, and tartary buckwheat, Food Chem. 300 (2019), 125189, https://doi.org/10.1016/j.foodchem.2019.125189.
[15] I.H. Said, R.L. Shah, M.S. Ullrich, N. Kuhnert, Quantification of microbial uptake of quercetin and its derivatives using an UHPLC-ESI-QTOF mass spectrometry assay, Food Funct. 7 (9) (2016) 4082–4091, https://doi.org/10.1039/C6FO00652C.
[16] F.A.O. Olgun, A. Üzer, B.D. Ozturk, R. Apak, A novel cerium oxide nanoparticles–based colorimetric sensor using tetramethyl benzidine reagent for antioxidant activity assay, Talanta 182 (2018) 55–61, https://doi.org/10.1016/j.talanta.2018.01.047.

[17] J. Alva-Ensastegui, M. Palomar-Pardavé, M. Romero-Romo, M. Ramírez-Silva, Quercetin spectrofluorometric quantification in aqueous media using different surfactants as fluorescence promoters, RSC Adv. 8 (20) (2018) 10980–10986, https://doi.org/10.1039/C8RA01213J.
[18] G. Weiz, J.D. Breccia, L.S. Mazzaferro, Screening and quantification of the enzymatic deglycosylation of the plant flavonoid rutin by UV–visible spectrometry, Food Chem. 229 (2017) 44–49, https://doi.org/10.1016/j.foodchem.2017.02.029.
[19] I.S. Lee, M.C. Boyce, M.C. Breadmore, Extraction and on-line concentration of flavonoids in Brassica oleracea by capillary electrophoresis using large volume sample stacking, Food Chem. 133 (1) (2012) 205–211, https://doi.org/10.1016/j.foodchem.2012.01.006.
[20] M. Tzanova, P. Peeva, Rapid HPLC method for simultaneous quantification of trans-resveratrol and quercetin in the skin of red grapes, Food Anal. Methods 11 (2) (2018) 514–521, https://doi.org/10.1007/s12161-017-1022-z.
[21] A. Canini, D. Alesiani, G. D'Arcangelo, P. Tagliatesta, Gas chromatography–mass spectrometry analysis of phenolic compounds from Carica papaya L. leaf, J. Food Compos. Anal. 20 (7) (2007) 584–590, https://doi.org/10.1016/j.jfca.2007.03.009.
[22] Y. Numata, H. Tanaka, Quantitative analysis of quercetin using Raman spectroscopy, Food Chem. 126 (2) (2011) 751–755, https://doi.org/10.1016/j.foodchem.2010.11.059.
[23] V.S. Chaudhari, R.M. Borkar, U.S. Murty, S. Banerjee, Analytical method development and validation of reverse-phase high-performance liquid chromatography (RP-HPLC) method for simultaneous quantifications of quercetin and piperine in dual-drug loaded nanostructured lipid carriers, J. Pharm. Biomed. Anal. 186 (2020), 113325, https://doi.org/10.1016/j.jpba.2020.113325.
[24] G.R. Vaz, A. Clementino, J. Bidone, M.A. Villetti, M. Falkembach, M. Batista, P. Barros, F. Sonvico, C. Dora, Curcumin and quercetin-loaded nanoemulsions: physicochemical compatibility study and validation of a simultaneous quantification method, Nanomaterials 10 (9) (2020) 1650, https://doi.org/10.3390/nano10091650.
[25] D. Shajari, A. Bahari, P. Gill, M. Mohseni, Synthesis and tuning of gold nanorods with surface plasmon resonance, Opt. Mater. 64 (2017) 376–383, https://doi.org/10.1016/j.optmat.2017.01.004.
[26] L. Tian, M. Su, F. Yu, Y. Xu, X. Li, L. Li, H. Liu, W. Tan, Liquid-state quantitative SERS analyzer on self-ordered metal liquid-like plasmonic arrays, Nat. Commun. 9 (2018) 3642, https://doi.org/10.1038/s41467-018-05920-z.
[27] T.K. Sau, C.J. Murphy, Seeded high yield synthesis of short Au nanorods in aqueous solution, Langmuir 20 (15) (2004) 6414–6420, https://doi.org/10.1021/la049463z.
[28] J.G. Mehtala, D.Y. Zemlyanov, J.P. Max, N. Kadasala, S. Zhao, A. Wei, Citrate-stabilized gold nanorods, Langmuir 30 (46) (2014) 13727–13730, https://doi.org/10.1021/la5029542.
[29] H.-Y. Ahn, H.-E. Lee, K. Jin, K.T. Nam, Extended gold nano-morphology diagram: synthesis of rhombic dodecahedra using CTAB and ascorbic acid, J. Mater. Chem. C 1 (41) (2013) 6861–6868, https://doi.org/10.1039/C3TC31135J.
[30] A. Ameer Abdullah, Maimoona Altaf, Hafsa Iktihar Khan, Gohar Ali Khan, Waqas Khan, Awais Ali, Arshad Saleem Bhatti, Sajid Ullah Khan, Waqqar, Facile room temperature synthesis of multifunctional CTAB coated gold nanoparticles, Chem. Phys. 510 (2018) 30–36, https://doi.org/10.1016/j.chemphys.2018.05.001.
[31] J.S. Komaiko, D.J. McClements, Formation of food-grade nanoemulsions using low-energy preparation methods: a review of available methods, Compr. Rev. Food Sci. Food Saf. 15 (2) (2016) 331–352, https://doi.org/10.1111/1541-4337.12189.
[32] V.S. Tiwari, T. Oleg, G.K. Darbha, W. Hardy, J. Singh, P.C. Ray, Non-resonance SERS effects of silver colloids with different shapes, Chem. Phys. Lett. 446 (1–3) (2007) 77–82, https://doi.org/10.1016/j.cplett.2007.07.106.
[33] E. Pinilla-Peñalver, M.J. Villaseñor, A.M. Contento, Á. Ríos, Erythrosine B – coated gold nanoparticles as an analytical sensing tool for the proper determination of both compounds based on surface-enhanced Raman spectroscopy, Microchem. J. 157 (2020), 104937, https://doi.org/10.1016/j.microc.2020.104937.
[34] M. Valcárcel, Á.I. López-Lorente, Gold Nanoparticles in Analytical Chemistry, Elsevier, 2014.
[35] R. Pilot, R. Signorini, C. Durante, L. Orian, M. Bhamidipati, L. Fabris, A review on surface-enhanced Raman scattering, Biosensors 9 (2) (2019) 57, https://doi.org/10.3390/bios9020057.
[36] M. Su, X. Li, S. Zhang, F. Yu, L. Tian, Y. Jiang, H. Liu, Self-healing plasmonic metal liquid as a quantitative surface-enhanced raman scattering analyzer in two-liquid-phase systems, Anal. Chem. 91 (3) (2019) 2288–2295, https://doi.org/10.1021/acs.analchem.8b04893.
[37] O. Kvítek, J. Siegel, V. Hnatowicz, V. Švorčík, Noble metal nanostructures influence of structure and environment on their optical properties, J. Nanomater. (2013), 743684, https://doi.org/10.1155/2013/743684.
[38] J.F. Arenas, J. Soto, I.L. Tocón, D.J. Fernández, J.C. Otero, J.I. Marcos, The role of charge-transfer states of the metal-adsorbate complex in surface-enhanced Raman scattering, J. Chem. Phys. 116 (16) (2002) 7207–7216, https://doi.org/10.1063/1.1450542.
[39] J. Cornard, J. Merlin, A. Boudet, L. Vrielynck, Structural study of quercetin by vibrational and electronic spectroscopies combined with semiempirical calculations, Biospectroscopy 3 (3) (1997) 183–193, https://doi.org/10.1002/(SICI)1520-6343(1997)3:3<183::AID-BSPY2>3.0.CO;2-7.
[40] P. Leyton, S. Sanchez-Cortes, M. Campos-Vallette, C. Domingo, J. Garcia-Ramos, C. Saitz, Surface-enhanced micro-Raman detection and characterization of calix [4] arene–polycyclic aromatic hydrocarbon host–guest complexes, Appl. Spectrosc. 59 (8) (2005) 1009–1015, https://doi.org/10.1366/0003702054615160.
[41] T. Wenzl, J. Haedrich, A. Schaechtele, P. Robouch, J. Stroka, Guidance Document on the Estimation of LOD and LOQ for Measurements in the Field of Contaminants in Feed and Food, Publications Office of the European Union: Luxemburg (2016) 58. https://doi.org/10.2787/8931.

Cristina Montes Ms.Sci. Degree in Analytical Chemistry. Ph.D. Student.

María Laura Soriano Associate Professor at the University of Córdoba (Spain).

María Jesús Villaseñor Assistant Professor in Analytical Chemistry at the University of Castilla – La Mancha (Spain).

Ángel Ríos Full Professor in Analytical Chemistry at the University of Castilla – La Mancha (Spain). Head of the research group on Simplification, Automation and Miniaturization of Analytical Processes.